Science of the Total Environment 787 (2021) 147586

Contents lists available at ScienceDirect

Science of the Total Environment

journal homepage: www.elsevier.com/locate/scitotenv

Smart sensors to predict entrainment of freshwater mussels: A new tool in freshwater habitat assessment

E.A.M. Curley [a,*], M. Valyrakis [b], R. Thomas [a], C.E. Adams [c], A. Stephen [d]

[a] School of Geographical and Earth Sciences, University of Glasgow, Glasgow, United Kingdom
[b] Infrastructure & Environment, James Watt School of Engineering, The University of Glasgow, Glasgow, United Kingdom
[c] Scottish Centre for Ecology & the Natural Environment, IBAHCM, University of Glasgow, Rowardennan, United Kingdom
[d] Scottish and Southern Energy, Perth, Perthshire, United Kingdom

HIGHLIGHTS

- Accessible approaches to record and monitor near-bed flow metrics remain undefined.
- Microelectromechanical sensors housed in mussel shells accurately detect movement.
- Recordings permit accurate detection and potential prediction of entrainment events.
- This tool could aid habitat suitability assessments for benthic aquatic species.
- Further study is required to assess its propensity to predict complex flow metrics.

GRAPHICAL ABSTRACT

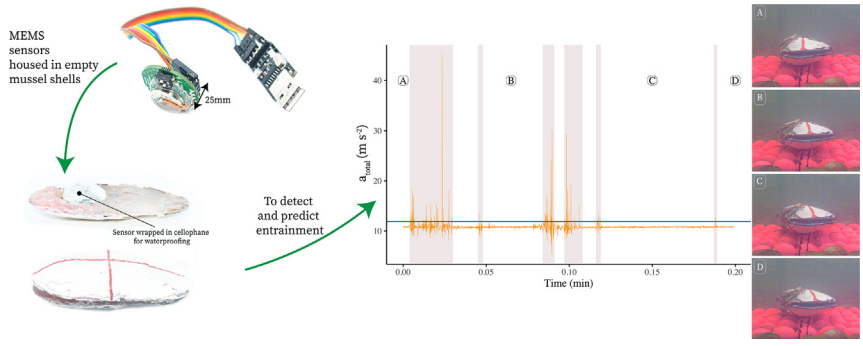

ARTICLE INFO

Article history:
Received 2 March 2021
Received in revised form 27 April 2021
Accepted 1 May 2021
Available online 13 May 2021

Editor: Henner Hollert

Keywords:
Inertial sensor
Frequency of entrainment
Habitat suitability
Unionid conservation
Instrumented shell
Hydraulic stressing

ABSTRACT

1. The quantification and assessment of dynamic hydrogeomorphological processes is crucial in defining suitable habitat for aquatic benthic species. Yet a consistent approach to accurately record and monitor near-bed flow characteristics, remains largely undefined in freshwater ecology.
2. The purpose of this work was to provide a direct, non-intrusive, low-cost and accessible tool to evaluate near-bed incipient flow conditions and predict when flow forcing results in the entrainment of individuals.
3. This study designed, for the first time, an instrumented freshwater mussel, encompassing inertial microelectromechanical sensors (MEMS), housed within *Margaritifera margaritifera* shells.
4. Following initial calibration of the embedded sensors to ensure accurate detection of three-dimensional displacement, dedicated flume experiments were undertaken to assess instrumented shell movement metrics, for a range of flow conditions and shell orientations.
5. Analysis found that data from the sensors' readings could successfully detect, and potentially predict, entrainment events through the examination of variability in recordings of total acceleration, with entrainment risk shown to vary across flowrate, shell orientation and size.
6. Instrumented shells could provide a valuable tool for assisting conservation management of freshwater mussel species: aiding the identification and monitoring of suitable habitat in reintroduction and restoration schemes. Instrumented shells could also assist habitat suitability surveys for a range of freshwater species, intimately linked to the physical environment of freshwater ecosystems.

* Corresponding author.
E-mail address: e.curley.1@research.gla.ac.uk (E.A.M. Curley).

https://doi.org/10.1016/j.scitotenv.2021.147586

7. Evidence from this study suggests further research into this tool may yield methods for accurately predicting more complex flow metrics associated with hydraulic stress. It is therefore clear that the potential of this tool is still to be fully investigated.

1. Introduction

The identification and protection of areas providing suitable habitat for species is crucial in the mitigation of biodiversity loss across ecosystems. Such methods are fundamental to conservation management in terrestrial and marine ecosystems, yet are often underutilised in efforts to conserve freshwater habitat (Decker et al., 2017; Moilanen et al., 2009). Considering that freshwater ecosystems represent some of the most threatened in the world, it is clear that more needs to be done to counteract the heightening extinction rate of species residing therein (Geist, 2011).

Efforts to bridge the gap between limited funding and the need for more extensive research, have led to calls for schemes to focus on keystone species, with the hope that their conservation will assist in inducing improvements to the health of the wider ecosystem (Bolotov et al., 2018). Freshwater unionid mussels (Mollusca: Bivalvia: Unionidae) are often considered important to ecosystem health by functioning as biomonitors of adverse habitat conditions (Lummer et al., 2016; Scheder et al., 2015; Vaughn, 2010); enhancing nutrient cycling and trophic interactions in freshwater communities (Allen et al., 2012; Boeker et al., 2016; Vaughn, 2010); and improving habitat diversity in benthic environments (Boeker et al., 2016; Spooner and Vaughn, 2008). Additionally, the biomass of unionids has been shown to often exceed that of all other benthic organisms in the habitat (Vaughn et al., 2004). Work by Geist (2010) suggested that one such species, the freshwater pearl mussel (*Margaritifera margaritifera*), fulfils the criteria for an indicator, flagship and keystone species. Despite their perceived importance, unionid mussels still represent some of the most imperiled species in the world (Lydeard et al., 2004).

Research concerning the habitat requirements of unionids is necessary to overcome limitations in conservation efforts (Boon et al., 2019; Cope et al., 2003; Geist, 2010), with Quinlan et al. (2015) highlighting the role of hydrogeomorphological processes, which govern habitat suitability within freshwater ecosystems, as an area requiring further attention. Hydraulic forcing has been shown to shape riverbed structure and composition (Biron et al., 2012; Crowder and Diplas, 2002a, b, 2006; Waddle and Holmquist, 2013), with potential implications towards habitat suitability for freshwater species that are intimately linked to their physical environment, such as *M. margartifera*; however, hydraulic stressing of freshwater mussels may be unique, and the response of mussels to alterations in flow has rarely been studied.

From a conservation perspective, entrainment incidents in populations of freshwater mussel species, resulting from high flow discharge, represent a clear threat to efforts to maintain and improve population health (Hardison and Layzer, 2001; Hastie et al., 2001; Hauer, 2015). Research by Hastie et al. (2001) highlighted the impact high flow events can have on unionid populations: reporting a 4–8% mortality (fifty thousand individuals) after a 1:100 year flood event, with juvenile mussels (<10 years old) disproportionately affected. Further study, regarding the role of high flows in shaping freshwater mussel populations, revealed an inhibition of juvenile settlement and a loss of stable substrates to facilitate burrowing (French and Ackerman, 2014; Randklev et al., 2019). It is likely that these events will occur more frequently and at greater magnitude in the future due to the effects of climate change (Cameron, 2006; Prudhomme et al., 2003; Schneider et al., 2013). There is, therefore, a need to understand and predict entrainment events towards detecting the presence of suitable habitat and identifying at-risk populations.

Studies attempting to link mussels with their physical and hydrodynamic habitat have rarely examined near-bed flow metrics; arguably the most ecologically relevant data for benthic biota, and often shown to be crucial in determining their spatial distribution (Blanckaert et al., 2013; Long et al., 2011; Oldmeadow et al., 2010; Robson et al., 1999). Instead, research has centred on correlative approaches towards determining abundance and distribution with hydraulic variables, or using predictive statistical models and computer simulations, with limited success: often attributed to inadequate flow data (limited range of measurements or a lack of direct measurements) (Gangloff and Feminella, 2007; Hardison and Layzer, 2001; Layzer and Madison, 1995; Morales et al., 2006).

Field studies that have examined near-bed flow characteristics, note a strong correlation between flow characteristics, such as shear stress, and mussel abundance, with data to suggest species-specific preference to hydrologic characteristics (Moorkens and Killeen, 2014; Stoeckl and Geist, 2016). However, field studies are often limited in their approach to accurately quantify near-bed flows, using methods reliant on single point measurements, which neglect variation in the flow dynamics across the riverbed (Crowder and Diplas, 2002a, b). The few laboratory-based studies that have quantified interactions between freshwater mussels and hydrodynamics, highlight the role of dense mussel beds in reducing near-bed flow velocity and altering the surrounding flow dynamics (Kumar et al., 2019; Sansom et al., 2020). Greater shell exposure has also been shown to elicit greater hydrodynamic stress to the individual (Sansom et al., 2018). Attempts to directly quantify mussel entrainment values (Thompson et al., 2016), reveal a potential interaction between substrate composition and structure, shell morphology, and individual behaviour; however, the experimental design of such studies limited the applicability of the results, with uncertainty concerning the reliability of flow measurements.

Recent advances in the prediction of turbulent flow conditions that evoke substrate particle entrainment have been made (Diplas et al., 2008; Valyrakis et al., 2010, 2013; Pähtz et al., 2020); however, these have yet to be applied to ecological studies. Rather, a dependency on indirect, time-consuming and often inaccurate methods for examining flow parameters and associated bed morphology persist: predictive models that attempt to understand the hydrodynamics of a river reach are often based on single point measurements (0.6 times flow height), compared across a limited range of flow conditions (Bey and Sullivan, 2015; Morales et al., 2006; Scheder et al., 2015); surveys to examine riverbed stability are founded on descriptive analyses, which risks substantial user-bias (Johnson and Brown, 2000; Schwendel et al., 2010). Attempts have been made to formalise methods for elucidating habitat suitability (Boon et al., 2019), yet accurate methods to record and monitor near-bed hydrogeomorphological characteristics remain undefined.

Recent technological advancements, concerning the use of inertial microelectromechanical sensors (MEMS), have enabled a deviation from traditional methods of monitoring surrogate flow metrics. Results from studies in the field of riverbed sediment transport suggest inertial sensors permit the direct assessment of sediment entrainment (Akeila et al., 2010; Gronz et al., 2016; Kularatna and Abeywardana, 2008; Valyrakis and Alexakis, 2016), with work by Al-Obaidi et al. (2020) demonstrating a link between logged readings and sediment entrainment based on derived performance indicators. However, research concerning entrainment risk to freshwater biota must consider the impact of behaviour and morphology, with organisms unlikely to respond

in a similar fashion to sediment particles when exposed to turbulent flows (Blanckaert et al., 2013; Kozarek et al., 2010).

The aim of this research was to adapt work with smart sensors from the field of riverbed sediment transport, and examine the suitability of inertial sensors to evaluate the incipient flow conditions at which unionid species are entrained from the riverbed surface; with the hope of providing a direct, non-intrusive, low-cost and accessible tool to assist conservation management in examining near-bed flow dynamics. The objectives were to design, for the first time, an instrumented freshwater mussel which comprises embedded inertial sensors within empty freshwater mussel shells, filled with silicone; to calibrate the instrumented shells, for different sizes, and test their functionality in a laboratory setting; to conduct dedicated flume experiments to assess instrumented shell movement metrics, for a range of flow conditions and initial orientations (fully exposed and partially buried); to analyse the experimentally obtained results towards identifying metrics that offer distinct criterion for assessing the risk to entrainment; and to validate the utility of this tool under identified metrics for indirectly assessing flow conditions that result in greater stressing of the mussels. We hypothesised that inertial microelectromechanical sensors (MEMS), housed within mussel shells, could provide an accurate method of identifying and predicting entrainment events. To our knowledge, this research would represent the first to employ such sensors for ecological assessment and identification of optimal habitat for a freshwater species.

2. Methodology

2.1. Defining entrainment of freshwater mussels

Initial work sought to define the theoretical modes of movement that would likely be observed for the two orientations that were to be studied (Fig. 1): fully exposed, resting horizontally on the bed surface; and partially buried, positioned vertically with 50% of the shell area submerged in the substrate.

For a fully exposed mussel, the key modes of entrainment were anticipated to be sliding and rolling (Valyrakis et al., 2010; Dey and Ali, 2018; Jain et al., 2020). For the partially buried mussel, the shell's asymmetrical shape may inhibit its removal from its pocket: the wider, heavier element was anchored below the surface, and the narrower part exposed to the flow (often orientated to streamline with the flow, as observed in live mussel beds); thus, hydrodynamic lift forces were expected to be less effective in displacing the mussel in a saltation mode (Wu and Chou, 2003; Diplas et al., 2008; Valyrakis et al., 2010; Dey and Ali, 2018). Instead, as the hydrodynamic forces increased, the shell was expected to move back and forth or sideways initially, until it repositioned itself into an orientation that enabled full entrainment out of its pocket as the experiment progressed (Valyrakis et al., 2010; Pähtz et al., 2020).

A partial or full entrainment event was expected to be dependent on the mode of movement, with a combination of modes expected to occur during an entrainment event. To quantify their occurrence, the conditions necessary to identify the presence and extent of each mode of movement were articulated. Critical values, which determined the presence or absence of a mode of movement, were based upon the minimal assessed displacements captured by high-speed video cameras, operating at 120 frames-per-second, that could be confirmed with a high degree of confidence.

For the fully exposed shell, three modes of movement were defined: a sliding movement (Fig. 1a), defined as a linear displacement along the x-axis of the shell, greater than or equal to 1 mm ($\Delta_x > \Delta_{x,c}$); a change of planar orientation (Fig. 1b), concerning movement around the z-axis, greater than or equal to 2° ($\Delta q_z > \Delta q_{z,c}$); and a rolling movement

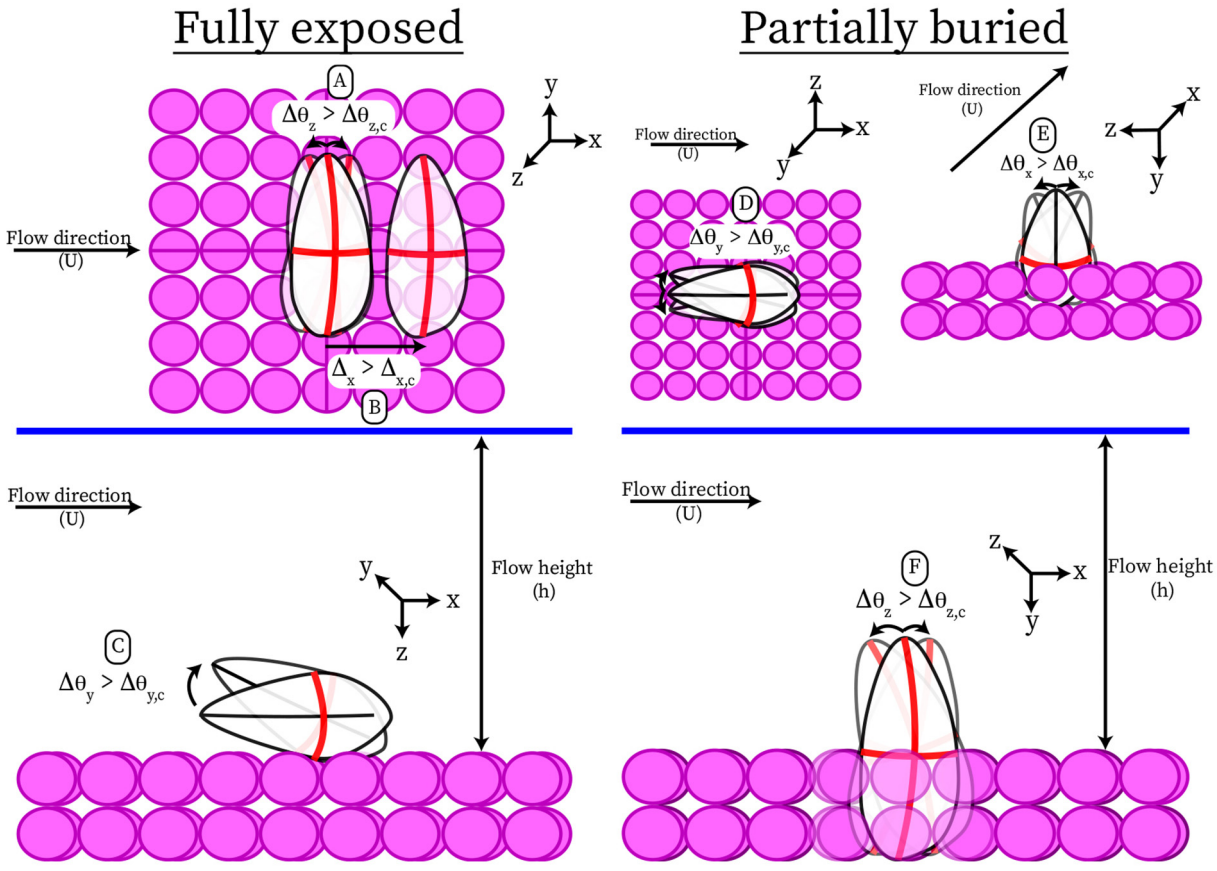

Fig. 1. The expected modes of movement to initiate partial or full entrainment for a mussel shell positioned in two orientations: horizontal on the bed, fully exposed to the flow (a–c); partially buried, with 50% of the shell area exposed to the flow (d–f).

(Fig. 1c), pertaining to an angular displacement of the shell around the y-axis, greater than or equal to 2° ($\Delta q_y > \Delta q_{y,c}$).

For the partially buried shell, three modes of movement were also defined: a change in planar orientation (Fig. 1d), which concerned movement around the y-axis, greater than or equal to 2° ($\Delta q_y > \Delta q_{y,c}$); a sideways movement relative to the flow (Fig. 1e), defined by an angular displacement around the x-axis, greater than or equal to 2° ($\Delta q_x > \Delta q_{x,c}$); and a forward or backward movement (Fig. 1f), categorised as an angular displacement around the z-axis, greater than or equal to 2° ($\Delta q_z > \Delta q_{z,c}$).

By articulating the method for quantifying the presence and magnitude for each mode of movement, output from the sensor could be used to accurately determine entrainment rates, which may serve as a metric to assess stress to freshwater mussels. Furthermore, validation of the sensor data by visual assessment of shell movement was improved, with camera positioning optimised to detect the pre-defined movements.

2.2. Considerations to sensor design

When outlining the design considerations and specifications that an inertial measurement unit must have to successfully identify these instances of entrainment at threshold flow conditions, the following were considered (Table S1): the size, shape and weight of the sensor; the availability and type of inertial sensor; the format for data transfer and storage; the energy supply and storage; the range of angular velocities and accelerations.

In response to the criteria (Table S1), Invensense MPU-9250 inertial sensors (Invensense Inc., San Jose, CA, USA) were selected for use in this research. This inertial sensor provides measurements concerning three-axis acceleration, three-axis rotational velocity, and three-axis magnetometer, in addition to an internal Digital Motion Processor, which supports up to 16 g of measurable acceleration, 2000° s^{-1} of measurable rotational velocity at an output frequency in excess of 200 Hz. With regards to data transfer and storage, discrete flash integrated circuits were selected for their predictable access, erase and write times, with the S25FL128S (Cypress Semiconductor Corporation, San Jose, CA, USA) specifically used due to its low unit cost, high data logging speed of 1.5 MB s^{-1} and 16 MB storage size. A serial converter to TTL 6-pin was used for charging and data transfer, ensuring a direct connection with the PC. An in-house Python code was developed to retrieve the data stored on the sensor's flash, which increased the speed of downloading the data to a PC substantially, with an hour of data logging requiring 3 min to download to a PC. The data was downloaded in an easy to use .csv format. In consideration of energy storage, rechargeable coin cells (Varta Microbattery produced under CoinPower, Varta Micorbattery GmbH, Ellwangen, Germany) were selected as cost-effective, practical alternatives to lithium batteries, and provided approximately 80 min of power from a single charge. For the final design of the sensor (Fig. S1), attention was paid towards ensuring the distribution of the mass across the instrumented shell was biologically relevant: similar to that of live mussels.

2.3. Design and creation of instrumented shell

Empty *M. margaritifera* shells from previously deceased individuals were collected from the South Esk River, Scotland, placed in bleach solution for 24 h and cleaned. Three shells, differing in size and morphology, were selected to function as instrumented shells, to represent a diversity in *M. margaritifera* size class: small; medium; and large (Table S2; Fig. S2b). To easily distinguish the instrumented shell from the surrounding bed, the outer area was painted white with aquarium-grade spray paint (Fig. S2a). For easy visual identification of shell motions, the central x-axis and y-axis of the shell were marked on the outer shell using red permanent marker, providing a high contrast colour to the white shell. Shells were filled with aquarium-grade silicone to a weight appropriate for the mussel size, accounting for the weight of the sensor (Fig. S2a). To house the sensor in the instrumented shell, a sensor was placed within a sealed impermeable cellophane wrap and pressed into the silicone before it had set to create an impression mould located on the intersection between the central x-axis and y-axis of the shell.

2.4. Calibration of instrumented shell

Two calibration tests were undertaken to examine how the data output from the sensor's triaxial gyroscope and accelerometer correlate with known changes in acceleration and rotation, when housed within the instrumented shell. The three shell sizes were used during the two calibration tests, to ensure there was no size dependent effects on the sensitivity of the data. For both calibration tests, the sensor was housed within the corresponding instrumented shell and placed on a non-slip craft mat (Fig. S3). The craft matt was divided into 10 mm × 10 mm squares. At the centre of the matt a circle (100 mm radius) was drawn with a marker pen, with 36 lines drawn from the centre of the circle to the perimeter, representing incremental changes in 10°. For both calibration tests, the instrumented shell was placed in the middle of the circle, with the shell aperture facing the 0° mark. To ensure continuity with the starting position, the instrumented shells were aligned as follows: the central x-axis of the shell aligned with the 180° and 0° line of the circle, whilst the central y-axis of the shell aligned with the 90° and 270° lines of the circle. Each calibration test for an instrumented shell comprised ten repeats of the same movement, with a repositioning back to the starting position at the end of each repeat.

Two high-speed video cameras operating at 120 frames-per-second (GoPro Hero 8 Black, Gopro, Inc., San Mateo CA, USA) were positioned to capture the instrumented shells' movement during the tests, to ensure accurate estimation of movement *via* a visual analysis. Both calibration tests were designed to mimic expected movement of the instrumented shell when experiencing significant hydraulic stress.

Data from the accelerometer and gyroscope were used to determine the total acceleration (Fig. 2) and total angular velocity respectively for the sensor using Eq. (1):

$$a = \sqrt{a_x^2 + a_y^2 + a_z^2} \quad (1)$$

where a_x, a_y and a_z are the x, y and z components of the acceleration, with ω_x, ω_x and ω_x, substituting the aforementioned as the x, y and z components of angular velocity when using the equation to calculate total angular velocity (ω; rad s^{-1}).

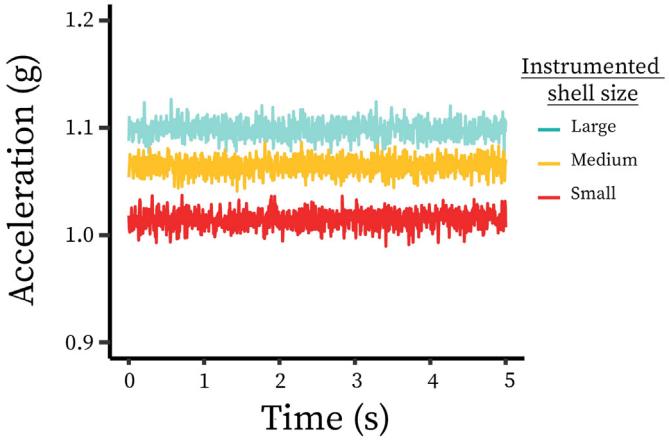

Fig. 2. Logged readings for total acceleration, recorded by the sensor's accelerometer during initial sensing check and endurance experiment.

2.4.1. Rotation around central axis

The first calibration test sought to reproduce a change of planar orientation ($\Delta q_z > \Delta q_{z,c}$) for a fully exposed mussel (Fig. 1a), concerning a 30° movement around the z-axis. To facilitate this movement, a cylindrical metal probe (length: 300 mm; circumference: 15.71 mm) was used to push the edge of the shell backwards, from its starting position, until the y-axis aligned with the 120° and 300° markings (Fig. S3b). To ensure rotation around the central axis, and to limit sliding of the shell, a metal pin was placed through the intersection of the shell's x-axis and y-axis, which punctured the craft mat. A marker was placed on each shell to allow for accurate repetition of the point of contact with the metal probe each time. An estimate of the angular velocity for each experimental repeat was made using Eq. (2):

$$\omega = \frac{\Delta\alpha}{t} \tag{2}$$

where ω represents angular velocity (rad s^{-1}), Δα is the change in angle and t is the time in which the angle change occurs. Total angular velocity was calculated from the sensor's gyroscope data. See Table S3 for calibration test results.

The average error, between the theoretical estimation of total angular velocity and the readings from the sensor, was 5.61% and deemed to be acceptably low considering the measurements were made by hand and the theoretical estimation is based on a smooth and consistent movement with no sliding, which could not be guaranteed.

2.4.2. Sliding along surface

The second calibration test sought to reproduce the sliding of a fully exposed shell along the x-axis in a linear displacement ($\Delta_x > \Delta_{x,c}$). Here, the cylindrical metal probe was modified, with a metal plate (135 mm × 30 mm × 5 mm) fixed to one end (Fig. S3c). The metal plate provided a flat surface to push the instrumented shell backwards, whilst minimising substantial changes in the angle of the shell. For each experimental repeat the metal probe pushed the shell backwards by 20 mm. An estimate of the acceleration for each experimental repeat was calculated using Eq. (3):

$$a = \frac{2s}{t^2} \tag{3}$$

where a represents acceleration (m s^{-2}), s is displacement (m), and t is time (s). Total acceleration was calculated from the sensor's accelerometer data. See Table S4 for calibration test results.

The average error, between the theoretical estimation of total acceleration and the readings from the sensor, was 4.86%, and deemed to be acceptably low considering the measurements were made by hand and the theoretical estimation is based on a smooth and consistent movement, which could not be guaranteed.

2.5. Examination of sensor operation

Sensing checks were undertaken to ensure the sensor adequately detected alterations in the movement of the instrumented shells, when housed within the shell, and submerged in water. Here, a sensor was wrapped in cellophane for waterproofing, and placed in each of the three instrumented shells, with the x-axis and y-axis of the sensor aligned with the central x-axis and y-axis of the shell. The shell was then placed within a glass aquarium tank (600 mm × 480 mm × 300 mm), on a substrate of fine gravel (0.5–4 mm) to a depth of 15 mm, and submerged in water to a depth of 300 mm. An Eheim Universal 1250 centrifugal pump was placed in the aquarium tank, 250 mm away from the instrumented shell's position, and connected to a timer switch, which ensured the pump cycled between 2 min of operation at an output of 1200 L h^{-1} and 2 min of rest. Two sensing checks were undertaken for each of the three instrumented shell sizes, for the two orientations (Fig. 1). The sequence for a sensing check was as follows: (1) sensor switched on and placed inside instrumented shell; (2) shell placed in aquarium tank either partially buried or fully exposed; (3) Eheim pump underwent three cycles of operation and rest; (4) pump switched off; and (5) instrumented shell removed from the tank, with sensor subsequently extracted and switched off. The resulting motion of the sensor was then checked, with readings from the accelerometer and gyroscope observed separately over the three axes. From the sensing checks, the ranges of 16 g and 2000° s^{-1} were deemed sufficient for recording the angular velocity and acceleration respectively, for the instrumented shells.

2.6. Flume set-up and test section

To further examine the application of the instrumented shells, experiments were conducted in a well-controlled 8 m long water recirculating flume, located at the Water Engineering Lab, University of Glasgow (Fig. 3a). The 0.9 m wide open channel supports flows of up to 0.4 m in depth, with water provided at a maximum capacity of 0.2 m^3 s^{-1}, controlled by a torque inverter to modify operational pump frequency. An adjustable tailgate, located at the outlet, permitted the maintenance of intended flow depths at reasonable flow velocities. To gain adequate hydraulic roughness, the bed surface comprised layers of water-worked uniformly sized fine gravel, with a median size of d_{50} = 15–25 mm, to a depth of 120 mm. Fine gravel was chosen to replicate the substratum conditions often highlighted as favourable for unionid mussels to burrow into (Geist and Auerswald, 2007; Hastie et al., 2000). A test section (1 m × 0.5 m) was located 5.7 m downstream of the channel inlet, 1.3 m from the outlet, to ensure hydraulically rough, turbulent flow was fully developed at the point of shell placement. The test section was positioned along the centreline of the flume, 0.2 m, from the flume's glass walls.

Within the test section, layers of gravel were replaced by a homogenous bed of 15.5 mm diameter marble spheres, which surrounded a rigid marble matrix, by a radius of 100 mm, from the edge of the matrix to the gravel bed. This homogenous local micro-topography assisted the development of flow near the instrumented particle, reducing the likelihood of significant flux in the near-bed flow dynamics, which may cause anomalies in the sensor reading. The marble matrix (140 mm × 140 mm × 50 mm) was formed by gluing layers of marbles together in a rectilinear well-packed arrangement, with a 3D printed plastic plate (140 mm × 140 mm × 10 mm) as a foundation (Fig. 3b). The matrix comprised four walls, of two marbles in depth, and three marbles high. A hollow region in the centre of the rectilinear arrangement accommodated loose marbles; enabling the burial of the instrumented shell. A second rectilinear structure was formed to create a plate (109 mm × 109 mm × 15.5 mm), to be placed on top of the hollow region of the matrix, forming a rigid bed micro topography to allow the horizontal placement of the instrumented shell. Underneath the marble matrix, resided a metal plate (140 mm × 140 mm × 20 mm) above a layer of fine gravel, to ensure the top of the matrix resided at the same depth as the surrounding bed of loose marble spheres, with a gradient to match the surrounding topography. The marble matrix was painted neon pink with an aquarium-grade spray paint, to distinguish it from the surrounding bed, and achieve high contrast with the instrumented shells. The central x-axis and y-axis of the marble matrix were marked using black permanent marker, to ensure consistent alignment of the shells before each experimental repeat, and easier visual identification of shell movement: highlighting when a deviation from the axis alignment of shell and matrix had occurred.

Two high-speed commercial video cameras operating at 120 frames-per-second (GoPro Hero 8 Black, Gopro, Inc. San Mateo CA, USA) were positioned to capture the instrumented shell's movement. The first, placed within the flume channel near the flume wall to avoid interference with the flow properties near the instrumented shell, filmed horizontally across the micro-topography. The second, positioned above the flume channel parallel to the bed, filmed the micro-topography below.

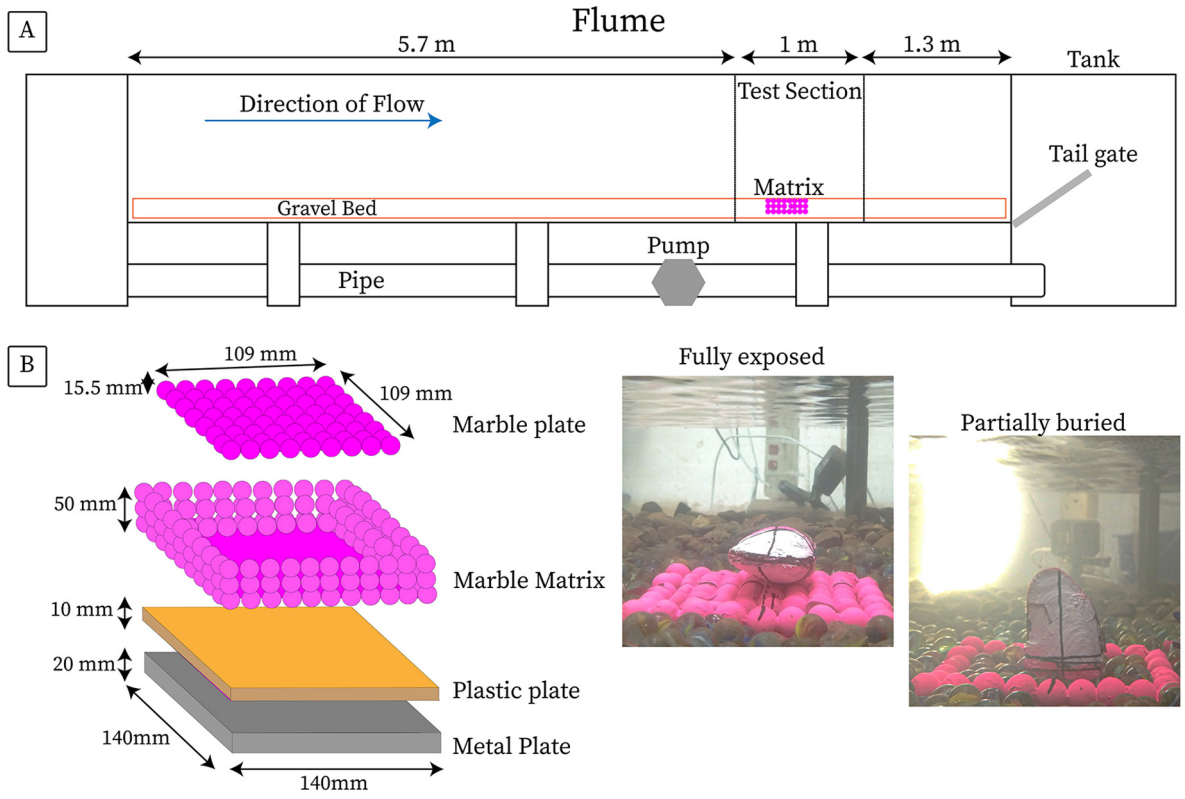

Fig. 3. The (A) experiment flume set-up, noting the location of the test section and marble matrix. Illustration of the (B) marble matrix structure, with photos to show the matrix accommodating the two orientations of instrumented shell.

A halo lamp was placed above the second camera to provide an ultra-bright light source.

2.7. Experimental protocol

2.7.1. Preparation of the shell

At the commencement of an experiment, the sensor was switched on and data logging enabled. The sensor was wrapped in layers of cellophane for waterproofing and positioned in the instrumented shell, with the sensor's x-axis aligned with that of the shell (Fig. S2a). The shell was then closed with small rubber bands to hold the two shell pieces together, and placed in a beaker at the base of a bucket, filled with water to a depth of 450 mm, and held for 2 min to allow trapped air to escape. The beaker was removed and weighed to record the shell's wet weight. The beaker was lowered into the flume, and the shell orientated according to predefined positioning criteria: (i) fully exposed, lying horizontally on the marble matrix with the shell aperture facing the flow, parallel to the bed, with the shell's central x-axis and y-axis aligned with that of the microtopography (Fig. 1); and (ii) partially buried, positioned vertically, with 50% of the shell buried in the loose marbles of the matrix, the shell aperture facing the flow, and the shell's y-axis perpendicular to that of the microtopography (Fig. 1).

2.7.2. Preliminary tests

Preliminary experiments were undertaken to detect the range of flow rates where the instrumented shell started becoming entrained, until the point at which the instrumented shell was difficult to maintain in its orientation during initial placement. Preliminary experiments were conducted for each of the three instrumented shell sizes. The instrumented shell was placed according to one of the two predefined positioning criteria. The flume was then run to provide an incremental increase in flowrate until mobilisation of the shell was observed and noted. Preliminary tests were repeated three times for each instrumented shell in a given orientation; thus, six preliminary tests were undertaken for each instrumented shell size.

2.7.3. Experimental tests

The experiment was designed to compare the response of the three instrumented shells across different flowrates, when positioned in two distinctive orientations, and examine whether these responses could be accurately correlated with readings from the accelerometer and gyroscope of the sensors housed therein.

Using data obtained from preliminary testing, three experimental flowrates were identified for each size of instrumented shell: High flowrate provided conditions known to induce frequent entrainment; Low flowrate comprised conditions where no shell movement was observed; Intermediate flowrate provided conditions where shell movement had occasionally been noted.

For each experiment, pump frequency was set and held at the predefined rate to provide conditions specific for a given size of instrumented shell and experimental flowrate (Table 1). After pump frequency was set, the flume was left undisturbed for 2 h to allow stable flow conditions to develop. Following this, flow height (h) was recorded using a digital depth gauge (Table 1), corresponding to the vertical distance from the water's edge to the top of a particle positioned in the experimental matrix (Fig. 1). To ensure consistency in recordings of flow height, the digital depth gauge was positioned on a circular mark, drawn onto a particle of the experimental matrix located 1 cm upstream of the instrumented shell in the centre of the flume channel (45 cm from the flume walls). The digital depth gauge was then removed and an Acoustic Doppler Velocimeter probe (ADV Vectrino II, Nortek AS, Rud, Norway) was then positioned at 0.6 times flow height, in its place, and recorded the flow velocity in the flume channel for 8 min (Table 1). The ADV probe was then removed before sensor measurements were taken.

Table 1
Recordings of mean flow velocity, flow height and Reynolds Number (Re) across the respective High, Intermediate and Low Experimental Flowrates for the three instrumented shell sizes.

Size	Mean flow velocity at 60% flow height ($m\ s^{-1}$)			Flow height (mm)			Reynolds number (*Re*)		
	High	Intermediate	Low	High	Intermediate	Low	High	Intermediate	Low
Large	0.147	0.102	0.053	142.63	135.82	115.07	20,883	13,798	6074
Medium	0.111	0.055	0.053	141.29	129.67	115.07	15,620	7103	6074
Small	0.107	0.055	0.053	140.20	129.67	115.07	14,941	7103	6074

The shell was placed according to one of the two predefined positioning criteria. Following a 2-minute incubation period, where the shell was left undisturbed, a ten-minute measurement period began. The instrumented shell was allowed to move from its initial positioning downstream, due to sufficiently energetic instantaneous near bed surface flow structures, with full entrainment from the test section permitted within a measurement period. At the end of a measurement period the shell was picked up, moved back and forth along its x-axis to provide a distinct fingerprint in the sensor data (indicating the end of an experimental repeat), and placed on the marble matrix, accordingly to the positioning criteria. Four further incubation and measurement periods followed to provide five replicates for one shell size, in one orientation, at a given experimental flowrate. At the end of an experiment, the sensor was removed from the shell, turned off and re-charged before data acquisition.

2.8. Data analysis

After each test, data was inputted into Matlab for further processing. Inverse uncertainty quantification was conducted using parameter calibration and data fusion. This filter accounts for the range of errors arising from the sensor's readings, quantified during the calibration process (Table S3; Table S4), and estimates final noise-corrected acceleration, angular velocity and orientation readings to be used in data analysis. The filter used a nine-axis Kalman filter structure (Kalman, 1960), incorporating inputs of expected accelerometer, gyroscope and magnetometer noise from the calibration tests to undertake the inertial sensor fusion filter.

3. Results and discussion

3.1. Initial data interpretation

After filtering the data, the results were used to calculate corrected total acceleration using Eq. (1). For each experiment, corrected total acceleration was compared with a visual analysis of the video data from the two cameras. Comparisons between the two data sources, enabled the identification of a threshold in the total acceleration data, pertaining to the occurrence of one, or multiple, modes of movement by the instrumented shell.

3.1.1. Calculating thresholds of entrainment

Initial analysis sought to evaluate whether data from the sensor could accurately and reliably detect modes of movement, which result in partial or full entrainment of the instrumented shell, when exposed to sufficient forcing from turbulent flow conditions (Fig. 4). For the

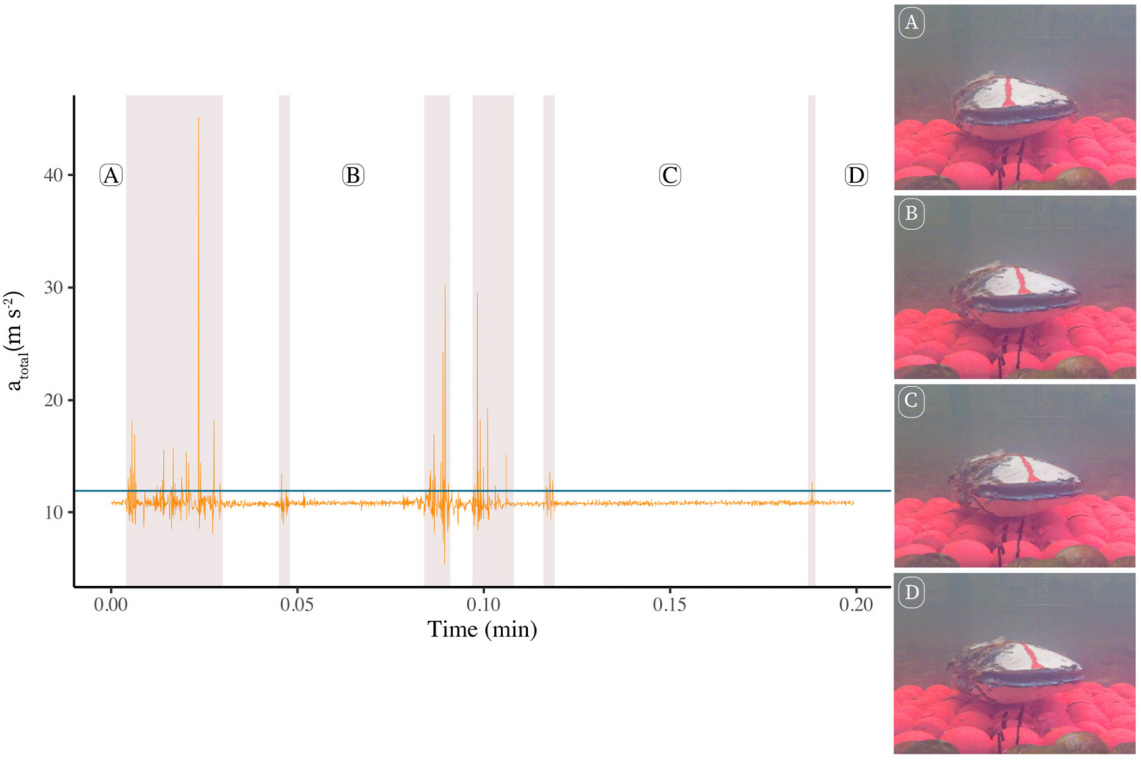

Fig. 4. Identification of entrainment events for fully exposed, large instrumented shell, during high experimental flowrate, using the fused sensor readings for total acceleration ($m\ s^{-2}$). Highlighted regions depict partial entrainment events. The thick blue line represents a threshold in total acceleration readings (average total acceleration ± 6*SD; 10.792 ± 0.708), above which partial entrainments could be visibly detected. Instrumented shell orientation is shown at four (A, B, C, D) periods within the time-series data, demonstrating a gradual change in planar orientation around the shell's z axis. (For interpretation of the references to colour in this figure legend, the reader is referred to the web version of this article.)

fully exposed Large instrumented shell, undergoing an experimental run with High experimental flow conditions, total acceleration values exceeding 11.38 m s^{-2} indicated a partial entrainment event (Fig. 4). Six partial entrainment events, defined by noticeable shifts in shell orientation without full displacement from the pocket, were identified (Fig. 4). The shell appeared to undergo a change of planar orientation around its z-axis. The first partial entrainment event occurred at 0.9 s and spanned a period of 1.32 s; depicting multiple peaks in the total acceleration, the most prominent of which occurred at 1.38 s with a maximum value of 45.109 m s^{-2}.

For each of the remaining five partial entrainment events (Fig. 4), significant increases in total acceleration from the sensor's readings (denoted by peaks in total acceleration typically exceeding 20 m s^{-2}) were shown to correlate with shifts in the instrumented particles' orientation. Thus, sensor readings for total acceleration appear to accurately convey movement in the instrumented shell. The data acquisition rate by the sensor and cameras are, therefore, sufficient for recording the modes of movement above the pre-defined critical values.

There were instances where energetic events, caused by turbulent flowing water, resulted in noticeable deviations from mean total acceleration readings; however, these were not forceful enough to generate instances where the critical value for a mode of movement was exceeded. These short-lived energetic events, insufficient in duration to result in any movement of the instrumented shell, were termed 'twitches' (Valyrakis et al., 2010).

Substantial shifts in shell movement, highlighted by peaks in total acceleration, were shown to position the shell in an orientation that incurs lesser forcing from the flow. Significant peaks in total acceleration were often greatest during the first entrainment event and rarely matched in magnitude later in an experimental repeat, with movement of the shell mimicking this trend: a substantial shift in orientation occurring initially, followed by smaller movements thereafter. This water-working of the shell, to a potentially more hydrodynamic orientation is similar to the process observed in riverbed substratum, whereby the onset of sediment transport is a continuous transition, from a creeping state to a granular flow (Houssais et al., 2015).

3.2. Entrainment frequency

The procedure for identifying thresholds in total acceleration to indicate entrainment events (Fig. 4), was applied to the results for all three instrumented shell sizes, across the respective High, Intermediate and Low experimental flowrates. Using the results from this analysis, the frequency of entrainment, f_E, was calculated for each experiment by dividing the total number of entrainment events recorded over the five experimental repeats by the total experimental time in seconds (Table 2). Analysis of these results revealed a difference in the frequency of entrainment across experimental flowrate, shell orientation and size.

For mussels positioned horizontally on the bed surface, fully exposed to the flow, the frequency of entrainment increased with increasing mean flow velocity (Fig. 5) across the three instrumented shell sizes, suggesting heightened flow rates induce increased rates of entrainment, irrespective of shell size. However, the extent to which f_E increases in response to increasing mean flow velocity is not consistent across the three instrumented shell sizes (Table 2).

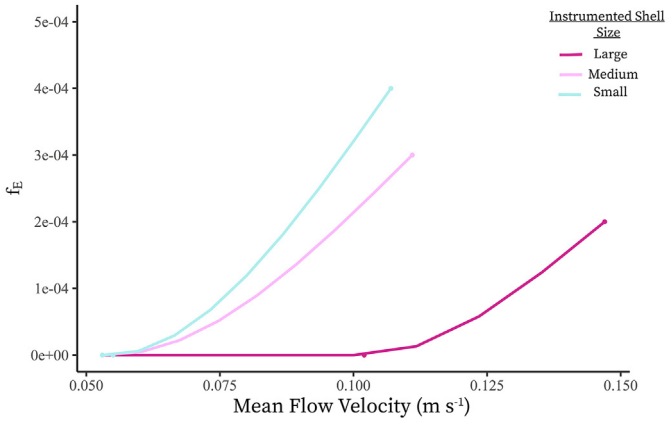

Fig. 5. Alterations in frequency of entrainment, f_E, associated with increasing mean flow velocity (m s^{-1}), for the three instrumented shell sizes, in the fully exposed orientation. Interpolation of the data points was undertaken using cubic Hermite spline.

Interpolation of the data (Fig. 5) revealed variation in readings of f_E when comparing the responses of the three instrumented shell sizes to the same flow conditions: at a mean flow velocity of 0.1 m s^{-1}, f_E was shown to be 50% higher in the Small instrumented shell compared to the Medium instrumented shell, with no entrainment events recorded for the Large instrumented shell. Therefore, smaller shell sizes appear more likely to be entrained than their larger counterparts, when exposed to the same flow conditions.

Comparisons of f_E during the High experimental flow rate conditions, for the respective instrumented shell sizes, revealed further variation in their responses: f_E was 33% higher in the Small instrumented shell compared to the Medium instrumented shell, despite a 3% increase in mean flow velocity; f_E was 100% higher in the Small instrumented shell compared to the Large instrumented shell, despite a 27% increase in mean flow velocity; f_E was 50% higher in the Medium instrumented shell compared to the Large instrumented shell, despite a 24% increase in mean flow velocity. Consequently, smaller shell sizes appear to display a more pronounced shift in f_E in response to increasing flowrate, with a larger shell size incurring a more gradual change in f_E in response to increasing flowrate.

Assessment of the effects of orientation on the risk of entrainment to the three instrumented shell sizes, revealed a complete absence of any modes of movement in the shells across the respective experimental flowrates when partially buried in the riverbed. Consequently, submerging the shell in the riverbed substratum may significantly reduce the risk of entrainment to the instrumented shell. Further research, with increased mean flow velocities, to induce greater stress from the flow are required to discern to what extent partial burial inhibits movement, and whether differences across shell sizes in this orientation are analogous to results shown for fully exposed instrumented shells.

Table 2
The frequency of entrainment (f_E) events for the three instrumented shell sizes, across the two orientations and three corresponding Experimental Flowrates. Differences in mean total acceleration (±SD) from the respective sensor reading are noted.

Size	Orientation	f_E (Hz)			Mean (±SD) total acceleration (m s^{-2}) from sensor's accelerometer readings		
		High	Intermediate	Low	High	Intermediate	Low
Large	Fully Exposed	0.0002	0	0	10.792 ± 0.118	10.714 ± 0.089	10.786 ± 0.075
	Partially Buried	0	0	0	9.534 ± 0.095	9.665 ± 0.069	9.683 ± 0.051
Medium	Fully Exposed	0.0003	0	0	10.350 ± 0.094	10.329 ± 0.077	10.454 ± 0.0747
	Partially Buried	0	0	0	9.737 ± 0.078	9.634 ± 0.050	9.729 ± 0.046
Small	Fully Exposed	0.0004	0	0	9.937 ± 0.094	9.929 ± 0.075	9.939 ± 0.073
	Partially Buried	0	0	0	9.546 ± 0.075	9.853 ± 0.049	9.906 ± 0.046

Despite an absence of entrainment for the partially buried shells (Table 2), analysis of the data would suggest that other metrics could be generated to quantify the stress experienced by instrumented shells when partially buried. For example, increasing variation around mean total acceleration, in response to increasing flowrate, was observed in all three sizes of instrumented shell, across both orientations (Table 2). For each size of instrumented shell, increasing variation in total acceleration appears to be most noticeable when comparing the Low and Intermediate experimental flowrates to the High flowrate (Fig. S4). The instrumented sensors therefore appear capable of providing evidence of hydraulic stress in the absence of visual examinations of shell movement.

Relevance to practical applications.

Partial or full entrainment, twitching and no entrainment were successfully detected using the total acceleration results after defining a threshold value, a result shared in similar studies (Al-Obaidi et al., 2020). For all three instrumented shell sizes, the threshold value for entrainment was set at six standard deviations from the mean total acceleration for the experiment; thus, highlighting a commonality in the extent of variation in total acceleration related to a partial or full entrainment event. Variation in total acceleration readings could, therefore, be utilised to predict the probability of shell entrainment.

Theories concerning the probability of entrainment of individual particles in the riverbed are well established in hydraulic engineering (Valyrakis et al., 2011). These probabilistic approaches suggest that the assessment of the frequency of entrainment of the most exposed particle should be sufficient to identify the risk of onset of scour before an event has occurred. Research by Al-Obaidi et al. (2020) reinforced this notion by demonstrating the use of instrumented particles for predicting the risk of scour initiation to assess water infrastructure hazards. Despite this, such practices have rarely been adopted in more ecologically orientated research. Ecological studies concerning habitat suitability from the perspective of substrate stability have often relied on visual categorisations of riverbed composition, correlated with flow metrics such as shear stress to predict sediment stability (Daraio et al., 2010; Morales et al., 2006). However, geomorphological and hydrological hazards, such as riverbed destabilisation, often develop at a rate that exceeds the capacity of practitioners to detect and respond with the use of current tools.

Data from this research has shown that the fusion of recordings from the inertial sensors, and the subsequent creation of metrics such as the frequency of entrainment, have the potential to provide performance indicators associated with bed stability and the risk for scour (Al-Obaidi et al., 2020). For this study, the instrumented shells were created using the shells of deceased *M. margaritifera*; consequently, such tools are likely to be well suited to applications in the field concerning the examination of potential entrainment risk in live mussel beds. Given the morphological similarities, instrumented shells could be placed in orientations that mimic the behaviour of live mussels *in-situ* and provide an indication of riverbed stability and the hydraulic stress individuals may be experiencing.

The use of instrumented shells is unlikely to be limited to the study of freshwater mussels, but instead could be applied to a wide range of freshwater species, intimately linked to their physical environment: close associations with substratum stability have been shown in many lotic organisms, ranging from algae and aquatic plants (Grabowski and Gurnell, 2016; Matthaei et al., 2003; Smith et al., 2009), to invertebrates (Nakano et al., 2018; Schwendel et al., 2010) and fish (Bey and Sullivan, 2015). The use of the instrumented shells highlighted in this research could, therefore, be useful in the assessment of freshwater habitats; providing a quantitative method to examine stability in near-bed habitat, which is crucial for the conservation of a plethora of species. However, there are limitations to the current study that should be addressed before this tool can be deployed by practitioners.

Applications of this tool, which directly address interactions between freshwater mussels and their surrounding hydrodynamic habitat, necessitate further work to account for greater variety in mussel behaviour. For example, differences in the extent of burial and alterations to orientation should be investigated to provide greater biological relevance to recordings. Additionally, live freshwater mussels utilise their foot to anchor themselves into the substratum, to improve resistance to flow forcing (Lewis and Riebel, 1984; da Silva Cândido and Romero, 2007). This is not accounted for in the current design of the instrumented shell. Consequently, recordings from the instrumented shell in a partially buried orientation may overestimate the stress from flow forcing for a corresponding live mussel. This issue is perhaps less pertinent for the fully exposed orientation, as live mussels in a similar orientation are unlikely to benefit from the utilisation of the foot to mitigate hydraulic stress. To compensate for the absence of a foot, the instrumented shell could be weighted disproportionally towards the umbo, as demonstrated by Thompson et al. (2016). Additional field studies with the instrumented shells are also necessary to test the utility of this tool in more heterogeneous hydrodynamic environment: in this study, conditions within the flume provided a relatively homogenous unidirectional flow, whereas near-bed flow patterns within a river system are more complex (Crowder and Diplas, 2002a, 2006).

3.2.1. Biological relevance

An evaluation of the biological relevance of these results appears to confirm the long-held understanding that freshwater mussels, such as *M. margaritifera*, may minimise their risk of entrainment by burying into substratum (Allen and Vaughn, 2009; Sansom, 2018). However, the effect of burial on the mitigation of entrainment risk may not be consistent across individuals: observed differences in f_E across the three sizes of instrumented shell when fully exposed, indicates that variation in shell morphology may impact the extent of stress experienced, in response to increasing flow forcing.

Previous studies suggest that interspecific differences in shell morphology may be driven by hydrological conditions, with species adapting their morphology to cope with turbulent flow dynamics, by developing shell characteristics that aid in the inhibition of displacement or the rapid re-positioning to a favourable orientation after dislodgement (Bartsch et al., 2010; Hornbach et al., 2010; Randklev et al., 2019; Watters, 1994). However, variation in shell morphology is also prevalent at the intraspecific level (Preston et al., 2010). Within this study, morphological differences were also shown for individuals from the same population, with measurements of Height, Width and Length not shown to scale linearly with increasing shell size (Table S2). Therefore, phenotypic variation in shell morphology may drive substantial differences in the extent to which individuals and populations can cope with similar levels of hydraulic forcing.

The utilisation of behaviours such as burial to mitigate the risk of entrainment, may be deployed to different extents across individuals, depending on their shell morphology. Results from this study suggest that individuals with similar morphological characteristics to the Small instrumented shell, may be less likely to move in their environment, because movement out of a partially buried position to a more exposed orientation significantly increases their risk of entrainment. Furthermore, such individuals may also bury themselves to a greater extent, with increased exposure found to heighten the risk of entrainment, compared to individuals with larger shell sizes. Consequently, the capacity of smaller mussels to utilise movement to respond to alterations in conditions, may be substantially reduced; thus, increasing their risk to unfavourable environmental conditions. This may explain why mussels form dense beds and remain relatively sedentary therein: dense beds (>25 mussels m^{-2}) generate flow environments that decrease the turbulent shear stresses acting to dislodge individuals, and increase food provision through the heightened suspension of microphytobenthos (Sansom et al., 2020; Widdows et al., 2009).

Expansion of this study to align with the recent work of Sansom et al. (2020), by placing instrumented shells together in replica mussel beds to investigate interactions between the hydraulic stress experienced by individuals and the surrounding hydrodynamic environment,

would assist in expanding knowledge concerning the motivation for forming these assemblages, and their role in governing spatial variation in freshwater mussel populations. Further work to accommodate greater phenotypic variation in shell morphology, over a broader range of hydraulic conditions with different extents of shell burial, may also allow for the disentanglement of these complex interactions. Data from such research could be particularly useful in assisting conservation management in highlighting populations most at risk to entrainment, in addition to identifying whether the morphological characteristics of individuals, designated for reintroduction schemes, are suited to the hydrological environment of the recipient habitats.

3.3. Key findings

This study is the first known attempt at adapting the use of smart sensors in the assessment of habitat suitability, with results to suggest a broad applicability of such a tool for a multitude of freshwater species. Here, instrumented shells, created by placing inertial sensors within the empty shells of deceased *M. margaritifera*, have enabled the successful direct identification, and potential prediction, of entrainment events through the examination of variability in recordings of total acceleration. This cost-effective, accessible tool is likely to be beneficial to practitioners seeking to identify and monitor suitable habitat for freshwater species, whilst also highlighting populations in need of conservation intervention. Furthermore, analysis of variation in total acceleration, beyond generating metrics for predicting entrainment, has provided evidence to suggest further study into this tool could yield methods for accurately predicting more complex flow metrics associated with hydraulic stress. It is therefore clear that the potential of this tool is still to be fully uncovered.

Supplementary data to this article can be found online at https://doi.org/10.1016/j.scitotenv.2021.147586.

Data access

The data that support the findings of this study are available from the corresponding author upon reasonable request.

Funding

This work was supported by a NERC iCASE studentship grant (NE/N007743/1), with funding from Scottish and Southern Energy (SSE) and the Scottish Alliance for Geoscience, Environment and Society (SAGES).

CRediT authorship contribution statement

E.A.M. Curley: Conceptualization, Methodology, Formal analysis, Investigation, Writing – original draft, Visualization. **M. Valyrakis:** Conceptualization, Validation, Methodology, Resources, Writing – review & editing. **R. Thomas:** Conceptualization, Writing – review & editing, Supervision, Project administration, Funding acquisition. **C.E. Adams:** Conceptualization, Supervision. **A. Stephen:** Supervision, Funding acquisition.

Declaration of competing interest

The authors declare that they have no known competing financial interests or personal relationships that could have appeared to influence the work reported in this paper.

Acknowledgements

Thanks to the technician, Timothy Montgomery, for his time and support in creating the experimental set-up. Thanks also to Khaldoon Al-Obaidi and Cameron Houston, for their guidance in the use of the sensors.

References

Akeila, E., Salcic, Z., Swain, A., 2010. Smart pebble for monitoring riverbed sediment transport. IEEE Sensors J. 10 (11), 1705–1717. https://doi.org/10.1109/JSEN.2010.2046726.

Allen, D.C., Vaughn, C.C., 2009. Burrowing behavior of freshwater mussels in experimentally manipulated communities. J. N. Am. Benthol. Soc. 28 (1), 93–100. https://doi.org/10.1899/07-170.1.

Allen, D.C., Vaughn, C.C., Kelly, J.F., Cooper, J.T., Engel, M.H., 2012. Bottom-up biodiversity effects increase resource subsidy flux between ecosystems. Ecology 93 (10), 2165–2174. https://doi.org/10.1890/11-1541.1.

Al-Obaidi, K., Xu, Y., Valyrakis, M., 2020. The design and calibration of instrumented particles for assessing water infrastructure hazards. J. Sens. Actuator Netw. 9 (3), 1–18. https://doi.org/10.3390/JSAN9030036.

Bartsch, M.R., Zigler, S.J., Newton, T.J., Sauer, J.S., 2010. Influence of shell morphology on distributions of unionids in the upper Mississippi River. J. Molluscan Stud. 76 (1), 67–76. https://doi.org/10.1093/mollus/eyp045.

Bey, C.R., Sullivan, S.M.P., 2015. Associations between stream hydrogeomorphology and co-dependent mussel-fish assemblages: evidence from an Ohio, USA river system. Aquat. Conserv. Mar. Freshwat. Ecosyst. 25 (4), 555–568. https://doi.org/10.1002/aqc.2539.

Biron, P.M., Carver, R.B., Carre, D.M., 2012. Sediment transport and flow dynamics around a restored pool in a fish habitat rehabilitation project: field and 3D numerical modelling experiments. River Res. Appl. 28, 926–939. https://doi.org/10.1002/rra.1488.

Blanckaert, K., Garcia, X.F., Ricardo, A.M., Chen, Q., Pusch, M.T., 2013. The role of turbulence in the hydraulic environment of benthic invertebrates. Ecohydrology 6 (4), 700–712. https://doi.org/10.1002/eco.1301.

Boeker, C., Lueders, T., Mueller, M., Pander, J., Geist, J., 2016. Alteration of physicochemical and microbial properties in freshwater substrates by burrowing invertebrates. Limnologica 59, 131–139. https://doi.org/10.1016/j.limno.2016.05.007.

Bolotov, I.N., Makhrov, A.A., Gofarov, M.Y., Aksenova, O.V., Aspholm, P.E., Bespalaya, Y.V., Kabakov, M.B., Kolosova, Y.S., Kondakov, A.V., Ofenböck, T., Ostrovsky, A.N., Popov, I.Y., Von Proschwitz, T., Rudzite, M., Rudzitis, M., Sokolova, S.E., Valovirta, I., Vikhrev, I.V., Vinarski, M.V., Zotin, A.A., 2018. Climate warming as a possible trigger of keystone mussel population decline in oligotrophic rivers at the continental scale. Sci. Rep. 8 (1), 1–9. https://doi.org/10.1038/s41598-017-18873-y.

Boon, P.J., Cooksley, S.L., Geist, J., Killeen, I.J., Moorkens, E.A., Sime, I., 2019. Developing a standard approach for monitoring freshwater pearl mussel (Margaritifera margaritifera) populations in European rivers. Aquat. Conserv. Mar. Freshwat. Ecosyst. 29 (8), 1365–1379. https://doi.org/10.1002/aqc.3016.

Cameron, D., 2006. An application of the UKCIP02 climate change scenarios to flood estimation by continuous simulation for a gauged catchment in the northeast of Scotland, UK (with uncertainty). J. Hydrol. 328 (1–2), 212–226. https://doi.org/10.1016/j.jhydrol.2005.12.024.

Cope, W.G., Hove, M.C., Waller, D.L., Hornbach, D.J., Bartsch, M.R., Cunningham, L.A., Dunn, H.L., Kapuscinski, A.R., 2003. Evaluation of relocation of unionid mussels to in situ refugia. J. Molluscan Stud. 69 (1), 27–34. https://doi.org/10.1093/mollus/69.1.27.

Crowder, D.W., Diplas, P., 2002a. Vorticity and circulation: spatial metrics for evaluating flow complexity in stream habitats. Can. J. Fish. Aquat. Sci. 59 (4), 633–645. https://doi.org/10.1139/f02-037.

Crowder, D.W., Diplas, P., 2002b. Vorticity and circulation: spatial metrics for evaluating flow complexity in stream habitats. Can. J. Fish. Aquat. Sci. 59 (4), 633–645. https://doi.org/10.1139/f02-037.

Crowder, D.W., Diplas, P., 2006. Applying spatial hydraulic principles to quantify stream habitat. River Res. Appl. 22 (1), 79–89. https://doi.org/10.1002/rra.893.

Daraio, J.A., Weber, L.J., Newton, T.J., 2010. Hydrodynamic modeling of juvenile mussel dispersal in a large river: the potential effects of bed shear stress and other parameters. J. N. Am. Benthol. Soc. 29 (3), 838–851. https://doi.org/10.1899/09-118.1.

Decker, E., Linke, S., Hermoso, V., Geist, J., 2017. Incorporating ecological functions in conservation decision making. Ecol. Evol. 7 (20), 8273–8281. https://doi.org/10.1002/ece3.3353.

Dey, S., Ali, S.Z., 2018. Review article: advances in modelling of bed particle entrainment sheared by turbulent flow. Phys. Fluids 30 (6). https://doi.org/10.1063/1.5030458.

Diplas, P., Dancey, C.L., Celik, A.O., Valyrakis, M., Greer, K., Akar, T., 2008. The role of impulse on the initiation of particle movement under turbulent flow conditions. Science 322 (5902), 717–720. https://doi.org/10.1126/science.1158954.

French, S.K., Ackerman, J.D., 2014. Responses of newly settled juvenile mussels to bed shear stress: implications for dispersal. Freshw. Sci. 33 (1), 46–55. https://doi.org/10.1086/674983.

Gangloff, M.M., Feminella, J.W., 2007. Stream channel geomorphology influences mussel abundance in southern Appalachian streams, U.S.A. Freshw. Biol. 52 (1), 64–74. https://doi.org/10.1111/j.1365-2427.2006.01673.x.

Geist, J., 2010. Strategies for the conservation of endangered freshwater pearl mussels (Margaritifera margaritifera L.): a synthesis of conservation genetics and ecology. Hydrobiologia 644 (1), 69–88. https://doi.org/10.1007/s10750-010-0190-2.

Geist, J., 2011. Integrative freshwater ecology and biodiversity conservation. Ecol. Indic. 11 (6), 1507–1516. https://doi.org/10.1016/j.ecolind.2011.04.002.

Geist, J., Auerswald, K., 2007. Physicochemical stream bed characteristics and recruitment of the freshwater pearl mussel (Margaritifera margaritifera). Freshw. Biol. 52 (12), 2299–2316. https://doi.org/10.1111/j.1365-2427.2007.01812.x.

Grabowski, R.C., Gurnell, A.M., 2016. Hydrogeomorphology-ecology interactions in river systems. River Res. Appl. 22, 1085–1095. https://doi.org/10.1002/rra.

Gronz, O., Hiller, P.H., Wirtz, S., Becker, K., Iserloh, T., Seeger, M., Brings, C., Aberle, J., Casper, M.C., Ries, J.B., 2016. Smartstones: a small 9-axis sensor implanted in stones to track their movements. Catena 142, 245–251. https://doi.org/10.1016/j.catena.2016.03.030.

Hardison, B.S., Layzer, J.B., 2001. Relations between complex hydraulics and the localized distribution of mussels in three regulated rivers. River Res. Appl. 17 (1), 77–84. https://doi.org/10.1002/1099-1646(200101/02)17:1<77::aid-rrr604>3.0.co;2-s.
Hastie, L.C., Boon, P.J., Young, M.R., 2000. Physical microhabitat requirements of freshwater pearl mussels, Margaritifera margaritifera (L.). Hydrobiologia 429, 59–71. https://doi.org/10.1023/a:1004068412666.
Hastie, L.C., Boon, P.J., Young, M.R., Way, S., 2001. The effects of a major flood on an endangered freshwater mussel population. Biol. Conserv. 98 (1), 107–115. https://doi.org/10.1016/S0006-3207(00)00152-X.
Hauer, C., 2015. Review of hydro-morphological management criteria on a river basin scale for preservation and restoration of freshwater pearl mussel habitats. Limnologica 50, 40–53. https://doi.org/10.1016/j.limno.2014.11.002.
Hornbach, D.J., Kurth, V.J., Hove, M.C., 2010. Variation in freshwater mussel shell sculpture and shape along a river gradient. Am. Midl. Natur. 164, 22–36.
Houssais, M., Ortiz, C.P., Durian, D.J., Jerolmack, D.J., 2015. Onset of sediment transport is a continuous transition driven by fluid shear and granular creep. Nat. Commun. 6, 1–8. https://doi.org/10.1038/ncomms7527.
Jain, R., Tschisgale, S., Fröhlich, J., 2020. Effect of particle shape on bedload sediment transport in case of small particle loading. Meccanica 55 (2), 299–315. https://doi.org/10.1007/s11012-019-01064-6.
Johnson, P.D., Brown, K.M., 2000. The importance of microhabitat factors and habitat stability to the threatened Louisiana pearl shell, *Margaritifera hembeli* (Conrad). Can. J. Zool. 78 (2), 271–277. https://doi.org/10.1139/z99-196.
Kalman, R.E., 1960. A new approach to linear filtering and prediction problems. J. Fluids Eng. Trans. ASME 82 (1), 35–45. https://doi.org/10.1115/1.3662552.
Kozarek, J.L., Hession, W.C., Dolloff, C.A., Diplas, P., 2010. Hydraulic complexity metrics for evaluating in-stream brook trout habitat. J. Hydraul. Eng. 136 (12), 1067–1076. https://doi.org/10.1061/(ASCE)HY.1943-7900.0000197.
Kularatna, N., Abeywardana, D.K., 2008. Use of motion sensors for autonomous monitoring of hydraulic environments. Proceedings of IEEE Sensors, pp. 1214–1217 https://doi.org/10.1109/ICSENS.2008.4716661.
Kumar, S.S., Kozarek, J., Hornbach, D., Hondzo, M., Hong, J., 2019. Experimental investigation of turbulent flow over live mussels. Environ. Fluid Mech. 19 (6), 1417–1430. https://doi.org/10.1007/s10652-019-09664-2.
Layzer, J.B., Madison, L.M., 1995. Microhabitat use by freshwater mussels and recommendations for determining their instream flow needs. Regul. Rivers Res. Manage. 10, 329–345. https://doi.org/10.1002/rrr.3450100225.
Lewis, J.B., Riebel, P.N., 1984. The effect of substrate on burrowing in freshwater mussels (Unionidae). Can. J. Zool. 62 (10), 2023–2025. https://doi.org/10.1139/z84-296.
Long, A., Ashe, W., Ravana, K., Simon, K.S., 2011. The effects of water velocity and sediment size on Acroneuria abnormis (Plecoptera: Perlidae) entrainment. Aquat. Insects 33 (2), 105–112. https://doi.org/10.1080/01650424.2011.597406.
Lummer, E.M., Auerswald, K., Geist, J., 2016. Fine sediment as environmental stressor affecting freshwater mussel behavior and ecosystem services. Sci. Total Environ. 571, 1340–1348. https://doi.org/10.1016/j.scitotenv.2016.07.027.
Lydeard, C., Cowie, R.H., Ponder, W.F., Bogan, A.E., Bouchet, P., Clark, S.A., Cummings, K.S., Frest, T.J., Gargominy, O., Herbert, D.G., Hershler, R., Perez, K.E., Roth, B., Seddon, M., Strong, E.E., Thompson, F.G., 2004. The global decline of nonmarine mollusks. BioScience 54 (4), 321–330. https://doi.org/10.1641/0006-3568(2004)054[0321:TGDONM]2.0.CO;2.
Matthaei, C.D., Guggelberger, C., Huber, H., 2003. Local disturbance history affects patchiness of benthic river algae. Freshw. Biol. 48 (9), 1514–1526. https://doi.org/10.1046/j.1365-2427.2003.01103.x.
Moilanen, A., Wilson, K.A., Possingham, H., 2009. Spatial Conservation Prioritization: Quantitative Methods and Computational Tools — UQ eSpace. Oxford University Press https://espace.library.uq.edu.au/view/UQ:188794.
Moorkens, E.A., Killeen, I.J., 2014. Assessing near-bed velocity in a recruiting population of the endangered freshwater pearl mussel (Margaritifera margaritifera) in Ireland. Aquat. Conserv. Mar. Freshwat. Ecosyst. 24 (6), 853–862. https://doi.org/10.1002/aqc.2530.
Morales, Y., Weber, L.J., Mynett, A.E., Newton, T.J., 2006. Effects of substrate and hydrodynamic conditions on the formation of mussel beds in a large river. J. N. Am. Benthol. Soc. 25 (3), 664–676. https://doi.org/10.1899/0887-3593(2006)25[664:EOSAHC]2.0.CO;2.
Nakano, D., Nagayama, S., Kawaguchi, Y., Nakamura, F., 2018. Significance of the stable foundations provided and created by large wood for benthic fauna in the Shibetsu River, Japan. Ecol. Eng. 120, 249–259. https://doi.org/10.1016/j.ecoleng.2018.05.032.
Oldmeadow, D.F., Lancaster, J., Rice, S.P., 2010. Drift and settlement of stream insects in a complex hydraulic environment. Freshw. Biol. 55 (5), 1020–1035. https://doi.org/10.1111/j.1365-2427.2009.02338.x.
Pähtz, T., Clark, A.H., Valyrakis, M., Durán, O., 2020. The physics of sediment transport initiation, cessation, and entrainment across Aeolian and fluvial environments. Rev. Geophys. 58, e2019RG000679. https://doi.org/10.1029/2019RG000679.
Preston, S.J., Harrison, A., Lundy, M., Roberts, D., Beddoe, N., Regowski, D., 2010. Square pegs in round holes — the implications of shell shape variation on the translocation of adult *Margaritifera margaritifera* (L.). Aquat. Conserv. Mar. Freshw. Ecosyst. 20, 568–573.
Prudhomme, C., Jakob, D., Svensson, C., 2003. Uncertainty and climate change impact on the flood regime of small UK catchments. J. Hydrol. 277, 1–23. https://doi.org/10.1016/S0022-1694(03)00065-9.
Quinlan, E., Gibbins, C., Malcolm, I., Batalla, R., Vericat, D., Hastie, L.C., 2015. A review of the physical habitat requirements and research priorities needed to underpin conservation of the endangered freshwater pearl mussel Margaritifera margaritifera. Aquat. Conserv. Mar. Freshwat. Ecosyst. 25 (1), 107–124. https://doi.org/10.1002/aqc.2484.
Randklev, C.R., Hart, M.A., Khan, J.M., Tsakiris, E.T., Robertson, C.R., 2019. Hydraulic requirements of freshwater mussels (Unionidae) and a conceptual framework for how they respond to high flows. Ecosphere 10 (12). https://doi.org/10.1002/ecs2.2975.
Robson, B.J., Chester, E.T., Davis, J.A., 1999. Manipulating the intensity of near-bed turbulence in rivers: effects on benthic invertebrates. Freshw. Biol. 42 (4), 645–653. https://doi.org/10.1046/j.1365-2427.1999.00506.x.
Sansom, B.J., Bennett, S.J., Atkinson, J.F., Vaughn, C.C., 2020. Emergent hydrodynamics and skimming flow over mussel covered beds in rivers. Water Resour. Res. 56 (8), 1–17. https://doi.org/10.1029/2019WR026252.
Sansom, Brandon J., 2018. Freshwater Mussels as Ecosystem Engineers: Modulation of Near-Bed Hydrodynamics Through Mussel-Flow Interactions. University at Buffalo.
Sansom, Brandon J., Atkinson, J.F., Bennett, S.J., 2018. Modulation of near-bed hydrodynamics by freshwater mussels in an experimental channel. Hydrobiologia 810 (1), 449–463. https://doi.org/10.1007/s10750-017-3172-9.
Scheder, C., Lerchegger, B., Flödl, P., Csar, D., Gumpinger, C., Hauer, C., 2015. River bed stability versus clogged interstitial: depth-dependent accumulation of substances in freshwater pearl mussel (Margaritifera margaritifera L.) habitats in Austrian streams as a function of hydromorphological parameters. Limnologica 50, 29–39. https://doi.org/10.1016/j.limno.2014.08.003.
Schneider, C., Laizé, C.L.R., Acreman, M.C., Flörke, M., 2013. How will climate change modify river flow regimes in Europe? Hydrol. Earth Syst. Sci. 17 (1), 325–339. https://doi.org/10.5194/hess-17-325-2013.
Schwendel, A.C., Death, R.G., Fuller, I.C., 2010. The assessment of shear stress and bed stability in stream ecology. Freshw. Biol. 55 (2), 261–281. https://doi.org/10.1111/j.1365-2427.2009.02293.x.
da Silva Cândido, L.T., Romero, S.M.B., 2007. A contribution to the knowledge of the behaviour of *Anodontites trapesialis* (Bivalvia: Mycetopodidae). The effect of sediment type on burrowing. Belg. J. Zool. 137 (1), 11–16.
Smith, J.S., Chandler, J., Rose, J., 2009. High spatial resolution data acquisition for the geosciences: kite aerial photography. Earth Surf. Process. Landf. 34, 155–161. https://doi.org/10.1002/esp.
Spooner, D.E., Vaughn, C.C., 2008. A trait-based approach to species' roles in stream ecosystems: climate change, community structure, and material cycling. Oecologia 158 (2), 307–317. https://doi.org/10.1007/s00442-008-1132-9.
Stoeckl, K., Geist, J., 2016. Hydrological and substrate requirements of the thick-shelled river mussel *Unio crassus* (Philipsson 1788). Aquat. Conserv. Mar. Freshwat. Ecosyst. 26 (3), 456–469. https://doi.org/10.1002/aqc.2598.
Thompson, F., Gilvear, D., Tree, A., Jeffries, R., 2016. Quantification of freshwater pearl mussel entrainment velocities and controlling factors; a flume study. River Res. Appl. 32 (6), 1179–1186. https://doi.org/10.1002/rra.2938.
Valyrakis, M., Alexakis, A., 2016. Development of a "smart-pebble" for tracking sediment transport. International Conference on Fluvial Hydraulics River Flow https://scholar.google.com/citations?user=PBVt_hUAAAAJ&hl=en#d=gs_md_cita-d&u=%2Fcitations%3Fview_op%3Dview_citation%26hl%3Den%26user%3DPBVt_hUAAAAJ%26citation_for_view%3DPBVt_hUAAAAJ%3Al7t_Zn2s7bgC%26tzom%3D0.
Valyrakis, M., Diplas, P., Dancey, C.L., Greer, K., Celik, A.O., 2010. Role of instantaneous force magnitude and duration on particle entrainment. J. Geophys. Res. Earth Surf. 115. https://doi.org/10.1029/2008jf001247.
Valyrakis, M., Diplas, P., Dancey, C.L., 2011. Entrainment of coarse grains in turbulent flows: an extreme value theory approach. Water Resour. Res. 47 (9), 1–17. https://doi.org/10.1029/2010WR010236.
Valyrakis, M., Diplas, P., Dancey, C.L., 2013. Entrainment of coarse particles in turbulent flows: an energy approach. J. Geophys. Res. Earth Surf. 118 (1), 42–53. https://doi.org/10.1029/2012JF002354.
Vaughn, C.C., 2010. Biodiversity losses and ecosystem function in freshwaters: emerging conclusions and research directions. BioScience 60 (1), 25–35. https://doi.org/10.1525/bio.2010.60.1.7.
Vaughn, C.C., Gido, K.B., Spooner, D.E., 2004. Ecosystem processes performed by unionid mussels in stream mesocosms: species roles and effects of abundance. Hydrobiologia 527 (1), 35–47. https://doi.org/10.1023/B:HYDR.0000043180.30420.00.
Waddle, T.J., Holmquist, J.G., 2013. Macroinvertebrate response to flow changes in a subalpine stream: predictions from two-dimensional hydrodynamic models. River Res. Appl. 29 (3), 366–379. https://doi.org/10.1002/rra.1607.
Watters, G.T., 1994. Form and function of unionoidean shell sculpture and shape. Am. Malacol. Bull. 11, 1–20.
Widdows, J., Pope, N.D., Brinsley, M.D., Gascoigne, J., Kaiser, M.J., 2009. Influence of self-organised structures on near-bed hydrodynamics and sediment dynamics within a mussel (Mytilus edulis) bed in the Menai Strait. J. Exp. Mar. Biol. Ecol. 379 (1–2), 92–100. https://doi.org/10.1016/j.jembe.2009.08.017.
Wu, F.C., Chou, Y.J., 2003. Rolling and lifting probabilities for sediment entrainment. J. Hydraul. Eng. 129 (2), 110–119. https://doi.org/10.1061/(asce)0733-9429(2003)129:2(110.